Synthesis of $In_{2-x}Ge_xO_3$ nanopowders for thermoelectric applications

Emmanuel Combe
Laboratoire CRISMAT, UMR 6508 CNRS-ENSICAEN, 14050 Caen Cedex, France; and Laboratoire LCIS-GREENMAT, University of Liège, Chemistry Institute B6, 4000 Liège (Sart-Tilman), Belgium Shekhar D. Bhame and Emmanuel Guilmeau[a)]
Laboratoire CRISMAT, UMR 6508 CNRS-ENSICAEN, 14050 Caen Cedex, France

Frédéric Boschini and Rudi Cloots
Laboratoire LCIS-GREENMAT, University of Liège, Chemistry Institute B6, 4000 Liège (Sart-Tilman), Belgium

Bulk ceramics $In_{2-x}Ge_xO_3$ have been synthesized in air by using citrate gel process. Nanoparticles of less than 20 nm have been synthesized through an accurate control of the processing parameters. X-ray diffraction and scanning electron microscopy studies confirmed that the solubility limit of Ge in In_2O_3 (x_ℓ) is very small and that additions of more than about 0.5 at.% Ge lead to the presence of $In_2Ge_2O_7$ inclusions. Thanks to a high interdispersion of metal ions and homogeneity in elemental composition of the nanopowders obtained by citrate gel process, well-dispersed $In_2Ge_2O_7$ secondary phases can be formed in the Ge-doped In_2O_3 matrix. An abrupt increase in the electrical conductivity and in the carrier concentration with x is observed in the monophasic region ($x < x_\ell$), whereas in the biphasic region ($x > x_\ell$), these values do not vary significantly. Similarly, the thermopower $|S|$ value is correlated to this variation decreasing as x increases for $x < x_\ell$. Above the solubility limit, the decrease in the lattice thermal conductivity is shown to be dependent on the presence of well-dispersed $In_2Ge_20_7$ secondary phases. The dimensionless figure of merit value is increased up to 0.3, thanks to electron doping and phonon scattering.

I. INTRODUCTION

Over the past decade, thermoelectric devices have been deeply studied as new no-waste energy sources.[1] Thermoelectric devices allow the direct transformation of a heat source into an electrical current (Seebeck effect), and vice versa (Peltier effect), without using mechanical moving parts. By this way, thermoelectric devices are high durability systems for cooling/heating capacity. These devices can be used for promising applications such as the recycling into electricity of the large lost heat energy produced by automobile, manufactories, or incinerators. The performance of a thermoelectric material is determined by the value of the dimensionless figure of merit, $ZT = S^2T/\rho\lambda$, where S is the Seebeck coefficient or thermopower, ρ the electrical resistivity, and λ the thermal conductivity. The ratio S^2/ρ corresponds to the power factor (PF). Present research efforts are focused on developing new materials with high figure of merit preferably close to 1 or higher.

In this context, oxides are being explored as suitable materials for thermoelectric applications at high temperature in air due to the high chemical stability at elevated operational temperatures. These materials have the additional advantage to be generally composed of nontoxic elements, contrary to certain conventional intermetallic compositions used in actual thermoelectric devices. Recently, we have shown that Ge-doped In_2O_3 bulk ceramics exhibit a great potential as n-type elements.[2] It was observed that the electrical conductivity of In_2O_3 is increased by one order of magnitude by Ge doping (0.5 at.%) and changes from a semiconducting to a semimetallic behavior, whereas a high n-type thermopower value is obtained at high temperature. It was also shown that the presence of secondary phases $In_2Ge_2O_7$ promotes a decrease in the total thermal conductivity. However, the increasing amount of these secondary phases, organized as large crown-like agglomerates, induces an increase in the porosity. The correlation between the microstructure and the thermoelectric properties is then quite complex and requires the design of homogeneous and dense composite microstructures.

For that purpose, soft chemistry techniques allow a high interdispersion of metal ions and significantly improve the homogeneity in structural and elemental composition of the powders. Soft chemistry techniques also allow to control the size, the morphology of particles, and to realize materials with extremely low doping rate. The obtained nanopowders have a high reactivity and lead usually to a reduction of the sintering

temperature.[3] By using different soft chemistry process such as coprecipitation, hydrothermal synthesis or sol-gel techniques, a variety of In_2O_3 nanoparticles with different structural and shape properties have been already produced.[4–6] Among these different techniques, the citrate gel process is a suitable technique for the synthesis of nanopowders, which exhibit a high structural homogeneity.[7] In the citrate gel process, the citric acid complexes metal salts in solution by its carboxyl groups COOH. This leads to the formation of stable metal complex, and by hindering the ions mobility and segregation, the different ions are well distributed at the atomic scale in a polymer network. By heating this polymer network, an amorphous precursor material is synthesized, and by increasing the thermal treatment (between 500 and 900 °C), the respective metal oxide is obtained.[8]

We have then studied the preparation and the thermoelectric properties of Ge-doped indium oxide ceramics prepared by the citrate gel process. The variation of the Seebeck coefficient, the electrical and thermal properties with temperature, and Ge content will be discussed and compared with those of $In_{2-x}Ge_xO_3$ ceramics prepared by conventional solid state chemistry.

II. EXPERIMENTAL

Indium nitrate [$In(NO_3)_2$, $5H_2O$ (99.99%, Alfa Aesar, Karlsruhe, Germany)], hexagonal germanium oxide GeO_2, and citric acid $C_6H_8O_7$ (Reactpur 100%) are used as starting materials. The preparation of the hexagonal germanium oxide is made by the precipitation of germanium chloride ($GeCl_4$, 99.9999%, Alfa Aesar) in deionized water. This leads to the formation of germanium hydroxide $Ge(OH)_2$, which is then evaporated for obtaining the hexagonal GeO_2 being soluble in water. $In_{2-x}Ge_xO_3$ powders were prepared by mixing stoichiometric amount ($2-x$:x:1) of the starting materials in deionized water under stirring. This solution is transferred into an alumina crucible and then heated up to 300 °C on hot plate for several hours to remove excess water. During this thermal treatment, a brown transparent colored gel is formed and then decomposed by self-combustion to a white foam powder. The dried precursor gel was then calcinated at 600 °C for 1 h with a heating rate of 100 °C/h.

Calcined powders mixed with polyvinyl alcohol binder were uniaxially pressed under 300 MPa. The polyvinyl alcohol is necessary for maintaining the shape of the green bulks after pressing. Parallelepiped $2 \times 3 \times 12$ mm^3 and cylindrical Ø20 $\times$ 4 samples were prepared. These samples were then sintered on platinum foils in an alumina crucible

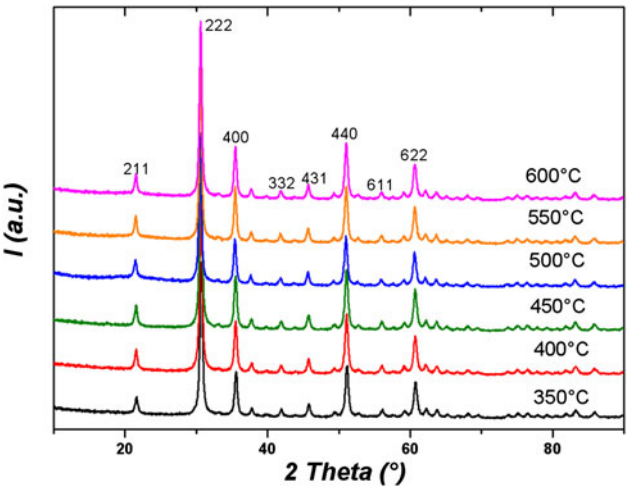

FIG. 2. X-ray diffraction (XRD) patterns of In_2O_3 powders calcined between 350 and 600 °C for 1 h.

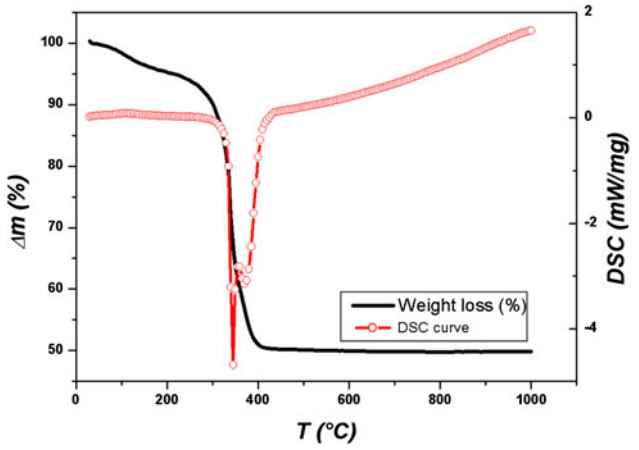

FIG. 1. Thermogravimetry and differential thermal analysis curves of the indium gel decomposition.

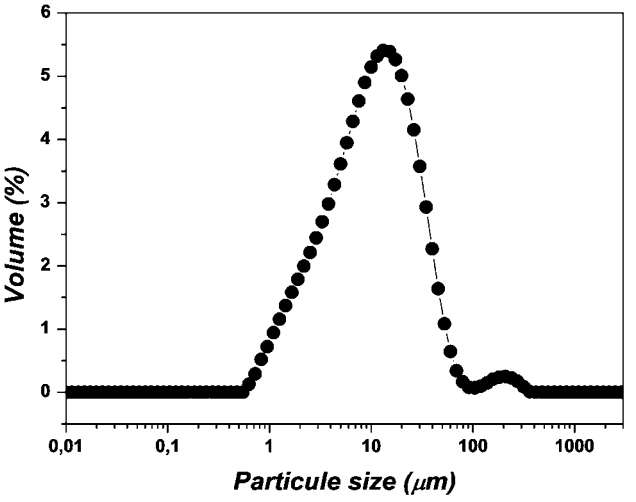

FIG. 3. Particle size distribution of In_2O_3 powder calcined at 600 °C during 1 h.

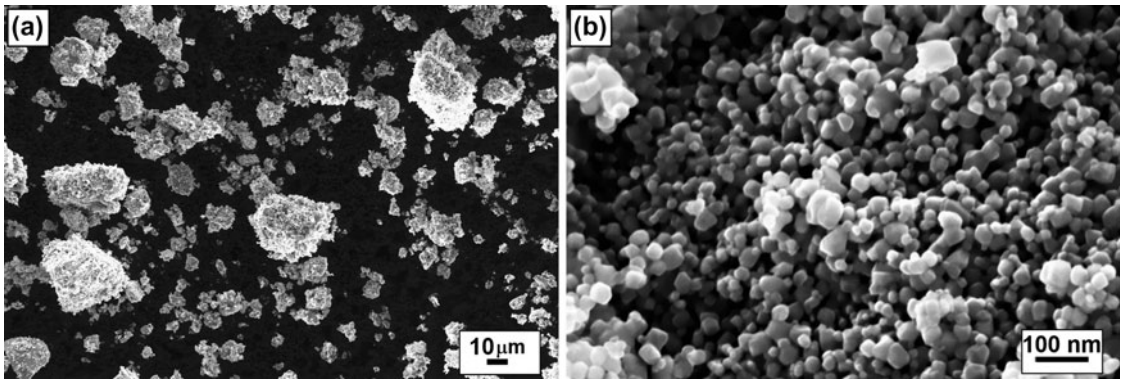

FIG. 4. Scanning electron microscopy (SEM) micrographs of In_2O_3 powder synthesized by citrate gel process and calcined at 600 °C during 1 h, for different magnifications (a and b).

at 1300 °C for 48 h. This thermal treatment was used for a direct comparison with $In_{2-x}Ge_xO_3$ realized by using solid state reaction.[2] The use of platinum foils is necessary for avoiding any contamination from the alumina crucible during sintering. The sintered pellets were then cut in square shape of 8 × 8 mm^2 to determine the thermal diffusivity.

Thermogravimetry and differential thermal analysis (TG/DTA) were carried out on a Netzsch Pegasus system (Netzsch, Selb, Germany). X-ray diffraction patterns (XRD) of the prepared $In_{2-x}Ge_xO_3$ powders were collected on a Philips X'Pert Pro diffractometer with X'Celerator (Philips, Almelo, Netherlands) using CuKα radiation in a 2θ range 10–90°. Rietveld refinement analysis (FullProf software)[9] were performed for the analysis of the XRD patterns. Particle size distribution was carried out by laser granulometry (Malvern Mastersizer 2000, Malvern, Orsay, France). Scanning electron microscopy (SEM) was performed on a FEG Zeiss Supra 55 (Carl Zeiss, Oberkochen, Germany). For this purpose, samples were polished until obtaining a mirror-like surface, and grain boundaries were then revealed by thermal etching at 1200 °C during 5 min. The measurements of the electrical resistivity and Seebeck coefficient were performed under partial helium pressure by using an ULVAC-ZEM3 device (Ulvac, Yokohama, Japan) from 300 to 1000 K. The thermal conductivity was determined by the product of the geometrical density, the heat capacity (Netzsch DSC 404C Pegasus), and the thermal diffusivity (Netzsch LFA457 MicroFlash). Hall effect experiments were performed as reported elsewhere.[10]

III. RESULTS AND DISCUSSION

Figure 1 shows the TG/DTA curves of the dried precursor after gel decomposition. A small weight loss (around 7%) is observed in the temperature range 100–200 °C indicating water evaporation. The second significant weight loss (about 40%) appears from 225 °C to around 400 °C with two endothermic peaks at 345 and 370 °C, in agreement with the results reported by Rey et al.[11] It can be attributed to

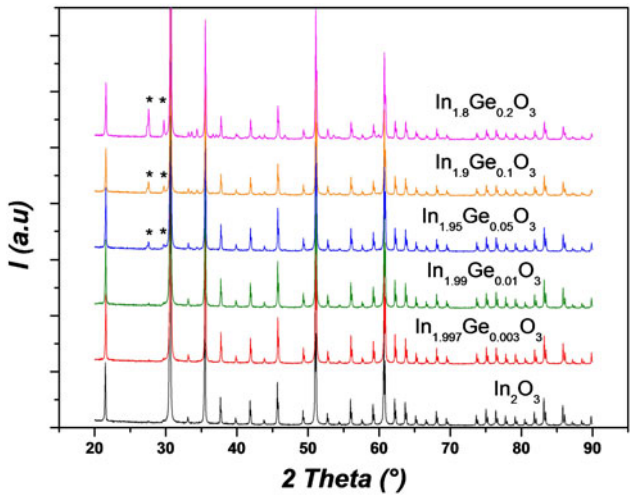

FIG. 5. XRD patterns of sintered $In_{2-x}Ge_xO_3$ ceramics (the symbols * indicate the presence of $In_2Ge_2O_7$ phases).

the decomposition of organic materials. Above 400 °C, the weight remains constant and no more endothermic or exothermic peaks are observed, which indicates that the crystallization of the indium oxide phase is achieved after a thermal treatment above 400 °C.

To investigate the changes in the average crystallites size of In_2O_3 particles resulting from the thermal decomposition of the dried precursor gel for temperatures higher than 400 °C, XRD measurements were carried out on different batches of indium oxide powders calcined at different temperatures between 350 and 600 °C for 1 h (Fig. 2). All diffraction patterns can be indexed with In_2O_3 Bragg reflections[12] and show no secondary phases or impurities. The width of peak at the half of the peak intensity does not show any variation with increasing temperature and indicates that the average size of crystallites is stable whatever the calcination temperature is. An average size of 20 nm has been determined by Rietveld refinement and Scherrer formula approximation.[9] The calcination temperature was then fixed to 600 °C during 1 h for all compositions to avoid any remaining organic

traces, which can prevent the densification of samples during sintering.

The Fig. 3 shows the particle size distribution of indium oxide powder after calcination. The apparent size distribution is broad (from 1 to 100 μm) with a maximum volume fraction centered on 10 μm which indicates an agglomeration of indium oxide nanoparticles. Micrometric agglomerates of In_2O_3 nanograins can be also observed on SEM micrographs in Figs. 4(a) and 4(b).

The XRD patterns of the sintered compounds with different Ge amounts are shown in Fig. 5. For Ge content higher than $x = 0.01$, several peaks corresponding to the $In_2Ge_2O_7$ phase are observed. This small Ge solubility limit in the In_2O_3 matrix was recently observed in $In_{2-x}Ge_xO_3$ samples obtained by solid state reaction.[2,10] The SEM micrographs of the different sintered samples are shown in Fig. 6. From $x = 0$ to $x = 0.01$, the porosity decreases (see Table I) and a slight grain growth is observed. Above the Ge solubility limit ($x = 0.01$), secondary phases appear and inner grain grows by diffusion scattering at grain boundaries. It must been noted that, contrary to $In_{2-x}Ge_xO_3$ samples prepared by solid state reaction, their distribution in the matrix is well homogeneous without any large empty sphere shapes.[2]

On the other hand, samples prepared by citrate gel process exhibit lower densification as compared with solid state reaction prepared samples. This is probably linked to the presence of agglomerates in the nanopowders prepared by the citrate gel process (as shown before). These results also suggest that the Ge for In substitution promotes an increase in the geometrical density of samples until the solubility limit. The

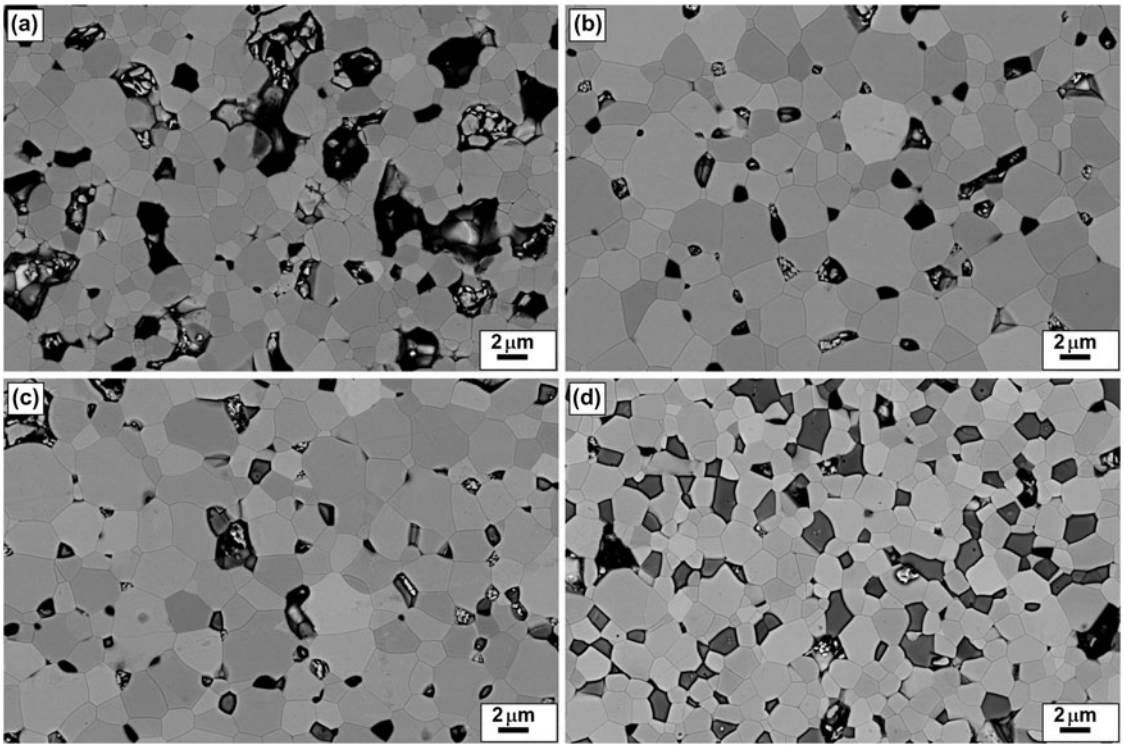

FIG. 6. SEM micrographs of sintered $In_{2-x}Ge_xO_3$ ceramics. The nominal compositions are: (a) In_2O_3, (b) $In_{1.99}Ge_{0.01}O_3$, (c) $In_{1.95}Ge_{0.05}O_3$, and (d) $In_{1.8}Ge_{0.2}O_3$. $In_2Ge_2O_7$ inclusions correspond to dark gray grains.

TABLE I. Geometrical density, carrier concentration (n), electrical resistivity (ρ), Hall mobility (μ), Seebeck coefficient (TEP), power factor (PF), thermal conductivity (λ), and ZT values in the $In_{2-x}Ge_xO_3$ series at 1000 K.

Ge content (x)	0	0.003	0.01	0.05	0.1	0.2
Relative density (%)	74	81	84	85	83	84
n ($\times 10^{20}$ cm^{-3}) at 300 K	0.70	0.83	1.53	1.96	1.71	1.15
μ (cm^2·V^{-1}·s^{-1}) at 300 K	31.6	52.8	41.6	37.4	29.8	28.7
ρ (mΩ·cm)	6.09	3.25	1.82	1.77	2.04	2.48
TEP (μV·K^{-1})	−169	−148	−116	−113	−114	−114
PF (mW·m^{-1}·K^{-2})	0.47	0.67	0.74	0.73	0.64	0.52
λ (W·m^{-1}·K^{-1})	2.19	2.31	3.28	3.06	2.97	2.00
ZT	0.21	0.29	0.22	0.24	0.22	0.26

geometrical density increases from 74% for $x = 0$ to 84% for $x = 0.01$. For higher Ge doping rate and contrary to $In_{2-x}Ge_xO_3$ samples prepared by solid state reaction, the geometrical density does not change and reaches about 84% of the theoretical density. It can be directly linked to the well dispersion of secondary phases in the matrix, as observed by SEM, and the absence of empty sphere secondary phases.

The temperature dependence of the electrical resistivity (Fig. 7) shows a linear increase characteristic to metal-like behavior. The electrical resistivity strongly decreases with increasing Ge content up to $x = 0.01$ (see for example at 1000 K in Table I). This drastic decrease is caused both by the increase in the geometrical density and in the carrier concentration (Table I). Above the solubility limit, the electrical resistivity increases due to the presence of $In_2Ge_2O_7$ insulating secondary phases. Concerning the carrier concentration of undoped In_2O_3, we can notice that this value ($n = 0.70 \times 10^{20}$ cm^{-3}) is higher than those reported in literature for In_2O_3 prepared by solid state reaction ($n = 0.11 \times 10^{20}$ cm^{-3}).[10] The use of the citrate gel process promotes a high reactivity of nanopowders and probably increases the presence of oxygen vacancies as additional donors.

The Hall mobility measured for the different samples (Table I) presents a maximum value for $x = 0.003$ ($\mu = 52.8$ cm^2·V^{-1}·s^{-1}). For $x \geq 0.003$, the Hall mobility decreases according to the increase in the carrier concentration until the solubility limit. This behavior is in agreement with results recently published for doped In_2O_3 bulks and thin films.[10,13] In a similar way with Sn/Ti/Zr-doped In_2O_3 compositions, the maximum Hall mobility for $In_{2-x}Ge_xO_3$ ceramics is obtained for low doping level ($x = 0.003$). Moreover, for a given x value, we observe a difference in the mobility for the Ge/Sn/Ti/Zr-doped In_2O_3 compositions. This difference may be linked to the influence of the difference of electronegativity and/or ionic radius of the doping metals on the interaction between substitutional ionized M^{z+} and electrons, and therefore the scattering rates. For higher substitution rate, the presence of ionized impurity scattering coupled with the increase in the carrier concentration promotes electron–electron scattering and leads to the decrease in the Hall mobility.

As shown in Fig. 7, the Seebeck coefficient has a negative value which indicates that the majority carriers are electrons. The absolute value of the Seebeck coefficient strongly decreases with the addition of germanium until the solubility limit (Table I). Above this limit of substitution and despite the presence of the $In_2Ge_2O_7$ secondary phases, the |S| does not change due to the fact that the thermopower is mainly linked to the matrix composition.[14] In Fig. 8, the temperature dependence of the PF is shown. For $x = 0$ to $x = 0.01$, the PF increases, respectively, from 0.47 to 0.74 mW·m^{-1}·K^{-2} at 1000 K

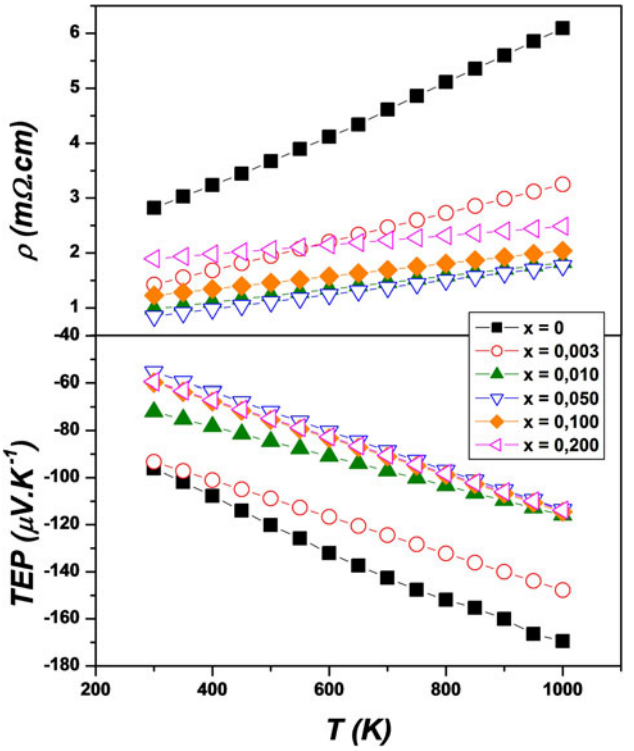

FIG. 7. Temperature dependence of the electrical resistivity and Seebeck coefficient (thermopower) of $In_{2-x}Ge_xO_3$ ceramics prepared by the citrate gel process.

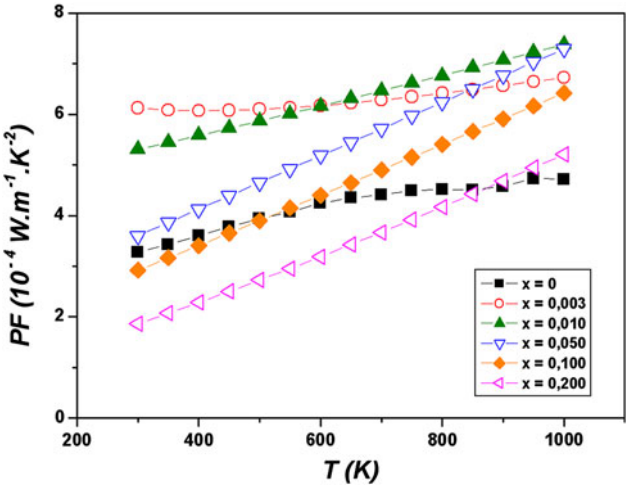

FIG. 8. Temperature dependence of the power factor in the series with nominal compositions $In_{2-x}Ge_xO_3$.

(Table I). At higher doping rates, the PF tends to decrease due to the increase in the electrical resistivity.

The temperature dependence of the thermal conductivity λ is shown in Fig. 9. For all samples, a decrease in the thermal conductivity with temperature is observed. According to the decrease in the electrical resistivity, the thermal conductivity is increasing with Ge doping level

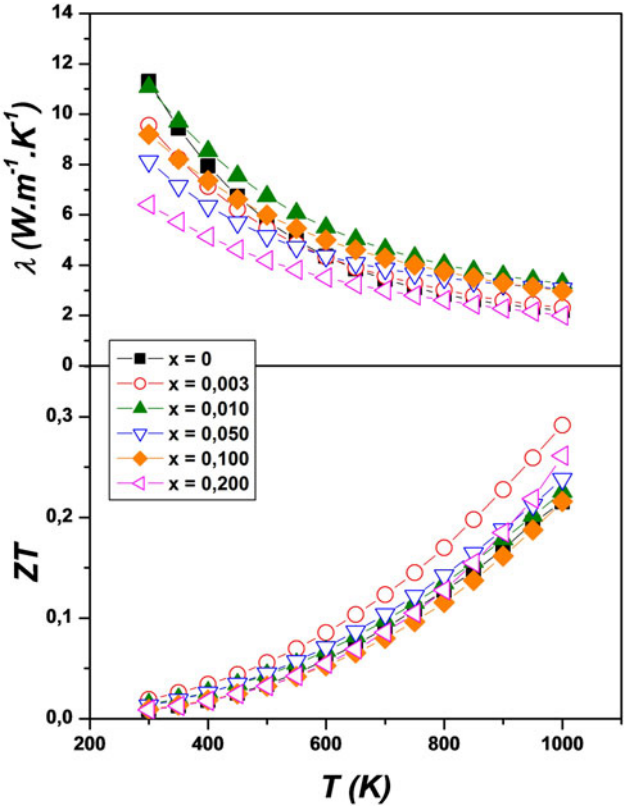

FIG. 9. Temperature dependence of the thermal conductivity and dimensionless figure of merit (ZT) in the series with nominal compositions $In_{2-x}Ge_xO_3$.

until the solubility limit, starting from 2.19 $W \cdot m^{-1} \cdot K^{-1}$ for $x = 0$ to 3.28 $W \cdot m^{-1} \cdot K^{-1}$ for $x = 0.01$ at 1000 K (Table I). Above the solubility limit, the thermal conductivity drastically decreases with Ge content and counterbalances the decrease in the PF. The calculated dimensionless figure of merit increases from 0.21 for In_2O_3 to 0.29 for $In_{1.997}Ge_{0.003}O_3$ and then remains almost stable up to $x = 0.2$. In contrary to $In_{2-x}Ge_xO_3$ processed by solid state chemistry,[2] the density remains constant above the solubility limit, thanks to the initial high interdispersion of metal ions, homogeneity in elemental composition of the nanopowders, and well dispersion of $In_2Ge_2O_7$ secondary phases. It can consequently access the comparison between thermal conductivity values measured on the different samples. The origin of the decrease in the thermal conductivity with high Ge doping level can be linked to the appearance of insulating $In_2Ge_2O_7$ secondary phases. It remains now to understand the origin of this effect, especially if any nanoscale effects due to the presence of defects or nanoinclusions can also exist and play any role in the transport properties of doped In_2O_3.

IV. CONCLUSION

The citrate gel process appears as a very suitable technique for the synthesis of Ge-doped indium oxide powders with nanosized grains. Although the germanium solubility limit is very small, the electrical resistivity of bulk sintered compounds is strongly decreased by doping, leading to high PFs, close to 1 $mW \cdot m^{-1} \cdot K^{-2}$ around 1000 K. Moreover, further Ge additions confirm the benefit role of well-dispersed $In_2Ge_2O_7$ phases for decreasing the overall thermal conductivity. The dimensionless figure of merit value is increased up to 0.3 at 1000 K, thanks to electron doping and phonon scattering.

REFERENCES

1. L.E. Bell: Cooling, heating, generating power, and recovering waste heat with thermoelectric systems. *Science* **321**, 1457 (2008).
2. D. Bérardan, E. Guilmeau, A. Maignan, and B. Raveau: In_2O_3:Ge, a promising n-type thermoelectric oxide composite. *Solid State Commun.* **146**, 97 (2008).
3. C.D.E. Lakeman and D.A. Payne: Sol-gel processing of electrical and magnetic ceramics. *Mater. Chem. Phys.* **38**, 305 (1994).
4. P. Xu, Z. Cheng, Q. Pan, J. Xu, Q. Xiang, W. Yu, and Y. Chu: High aspect ratio In_2O_3 nanowires: synthesis, mechanism and NO_2 gas-sensing properties. *Sens. Actuators, B* **130**, 802 (2008).
5. K.Y. Kim and S.B. Park: Preparation and property control of nano-sized indium tin oxide particle. *Mater. Chem. Phys.* **86**, 210 (2004).
6. G. Neri, A. Bonavita, G. Micali, G. Rizzo, N. Pinna, and M. Niederberger: In_2O_3 and Pt-In_2O_3 nanopowders for low temperature oxygen sensors. *Sens. Actuators, B* **127**, 455 (2007).
7. C. Marcilly, P. Courty, and B. Delmon: Preparation of highly dispersed mixed oxides and oxide solid solutions by pyrolysis of amorphous organic precursors. *J. Am. Ceram. Soc.* **53**, 56 (1970).
8. S. Ananthakumar, S. Anas, J. Ambily and R.V. Mangalaraja: Microwave assisted citrate gel combustion synthesis of ZnO. Part-1: assessment of structural features. *J. ceram. Process. Res.* **11**, 29 (2010).
9. J. Rodríguez-Carvajal: Recent advances in magnetic structure determination by neutron powder diffraction. *Physica B* **192**, 55 (1993).
10. E. Guilmeau, D. Bérardan, Ch. Simon, A. Maignan, B. Raveau, D.O. Ovono, and F. Delorme: Tuning the transport and thermoelectric properties of In_2O_3 bulk ceramics through doping at In-site. *J. Appl. Phys.* **106**, 053715 (2009).
11. J.F.Q. Rey, T.S. Plivelic, R.A. Rocha, S.K. Tadokoro, I. Torriani, and E.N.S. Muccillo: Synthesis of In_2O_3 nanoparticles by thermal decomposition of a citrate gel precursor. *J. Nanopart. Res.* **7**, 203 (2005).
12. M. Marezio: Refinement of the crystal structure of In_2O_3 at two wavelengths. *Acta Crystallogr.* **20**, 723 (1966).
13. M.F.A.M. van Hest, M.S. Dabney, J.D. Perkins, D.S. Ginley, and M.P. Taylor: Titanium-doped indium oxide: a high-mobility transparent conductor. *Appl. Phys. Lett.* **87**, 032111 (2005).
14. D.J. Bergman and O. Levy: Thermoelectric properties of a composite medium. *J. Appl. Phys.* **70**, 6821 (1991).